A&A 619, A62 (2018)
https://doi.org/10.1051/0004-6361/201833723

Astronomy & Astrophysics

Exploring the space density of X-ray selected cataclysmic variables

A. D. Schwope

Leibniz-Institut für Astrophysik Potsdam (AIP), An der Sternwarte 16, 14482 Potsdam, Germany
e-mail: aschwope@aip.de

Received 26 June 2018 / Accepted 21 August 2018

ABSTRACT

The space density of the various classes of cataclysmic variables (CVs) has up to now only been weakly constrained, due to the small number of objects in complete X-ray flux-limited samples and the difficulty in deriving precise distances to CVs. The former limitation still exists. Here the impact of *Gaia* parallaxes and implied distances on the space density of X-ray-selected complete, flux-limited samples is studied. These samples have been described in the literature: Those of non-magnetic CVs are based on ROSAT (RBS – ROSAT Bright Survey & NEP – North Ecliptic Pole) and that of the intermediate polars (IPs) stems from *Swift*/BAT. All CVs appear to be rarer than previously thought, although the new values are all within the errors of past studies. Upper limits at 90% confidence for the space densities of non-magnetic CVs are $\rho_{\rm RBS} < 1.1 \times 10^{-6}\,{\rm pc}^{-3}$ and $\rho_{\rm RBS+NEP} < 5.1 \times 10^{-6}\,{\rm pc}^{-3}$ for an assumed scale height of $h = 260\,{\rm pc}$ and $\rho_{\rm IPs} < 1.3 \times 10^{-7}\,{\rm pc}^{-3}$ for the long-period IPs at a scale height of 120 pc. Most of the distances to the IPs have previously been under-estimated. The upper limits to the space densities are only valid in cases where CVs do not have lower X-ray luminosities than the lowest-luminosity member of the sample. These results require confirmation using larger sample sizes, soon to be established through sensitive X-ray all-sky surveys to be performed with eROSITA on the Spektrum-X-Gamma mission.

Key words. novae, cataclysmic variables – surveys – X-rays: binaries

1. Introduction

The space density of cataclysmic variable stars (CVs) is one of the bigger unknowns in the field. Being the outcome of binary star evolution through a common envelope and subsequent angular momentum loss, this value is important for several parameters and processes that are relevant to binary evolution, including the initial binary separation, the initial mass distribution, the common envelope efficiency, and the angular momentum loss in the post-common envelope phase and that in the CV stage. It is the most relevant value to compare with binary population synthesis. The simple question is: how many CVs are out there?

This question is relevant for stellar evolution but has implications for models of the total energy output of the Milky Way. One of the contenders to explain the infamous Galactic ridge X-ray emission (GRXE, Worrall et al. 1982) is CVs and in particular magnetic CVs of the intermediate polar type (IPs). Through a deep *Chandra* pointing close to the galactic centre, the apparently diffuse GRXE was largely resolved into point sources (Revnivtsev et al. 2009). The composition however remained uncertain and was discussed thoroughly in the recent past and sensitively depends on the space density and the luminosity functions of the main source classes (e.g. Warwick 2014; Nobukawa et al. 2016).

The second data release from the *Gaia* satellite (*Gaia* DR2) opens the opportunity to re-assess the space density of X-ray-selected cataclysmic variables. Past studies were hampered by small sample sizes and imprecisely determined distances. While the former limitation cannot presently be overcome, the latter has essentially vanished.

In this paper the non-magnetic CVs (dwarf nova and nova-like systems) and one class of the magnetic CVs, the IPs, are addressed. Both sub-classes have relatively well-understood X-ray spectra which results in a relatively clean selection of objects. The strongly magnetic CVs, the polars, are not addressed here. Polars are special due to their more complex X-ray spectra with a thermal plasma and a potentially strong soft component. ROSAT has uncovered many soft blackbody-like polars (Beuermann & Schwope 1994), but all new discoveries made with *XMM-Newton* lack the pronounced soft component (see e.g. Webb et al. 2018, and references therein). Whether or not the observed sample of polars can be regarded as representative of the parent population is therefore questionable.

2. Analysis

2.1. Basic assumptions

In the following we derive space densities for X-ray-selected samples of CVs. The samples are described in the literature and no new sample composition was undertaken. We make three basic assumptions per case: that the observed sample is representative of the intrinsic population, the sample is complete, and that the sample is flux-limited with a well-defined flux-limit. For further details, see for example Pretorius & Knigge (2012).

For the analyses in the following sections we make use of parallaxes that were found by archival cone searches in the *Gaia* archive using data from *Gaia* DR2[1]. In case of multiple matches, the entry with the best matching brightness value was chosen. We do not invert parallaxes to infer distances but use the probabilistic distance estimates provided by Bailer-Jones et al. (2018)[2]. However, since most new parallaxes have very small relative errors, the use of directly inverted parallaxes gives almost the same results.

[1] https://gea.esac.esa.int/archive/
[2] http://gaia.ari.uni-heidelberg.de/tap.html

Table 1. Non-magnetic CVs found in the RBS.

RBS#	Name	$\widetilde{D}$ (pc)	$\widetilde{\log L_X}$ (s^{-1})	f_X (erg cm^{-2} s^{-1})	p (mas)	Δp (mas)	$\log L_X$ (s^{-1})	D (pc)	D_{max} (pc)	V_{gen} (pc^3)
2	EF Tuc	500:	32.0	3.38E–12	0.720	0.023	32.9	1335	1462	2.09E+08
22	WW Cet	100	31.0	9.16E–12	4.588	0.047	31.7	216	389	3.28E+07
280	TT ARI	135	31.1	5.96E–12	3.884	0.070	31.7	256	372	4.20E+07
288	WX HYI	265	31.6	6.26E–12	4.273	0.029	31.6	232	346	3.21E+07
372	IQ Eri	130	30.8	3.76E–12	5.186	0.167	31.2	192	222	1.11E+07
490		33	29.6	3.36E–12	3.098	0.126	31.6	320	349	3.51E+07
512	VW Hyi	65	30.9	1.59E–11	18.531	0.022	30.7	54	128	3.26E+06
664	TW Pic	–	–	3.13E–12	2.284	0.022	31.8	432	455	7.99E+07
694	SU UMa	280	32.1	1.41E–11	4.535	0.029	31.9	219	490	9.25E+07
710	SW UMa	140	30.9	3.81E–12	6.148	0.080	31.1	162	188	9.09E+06
(713	EI UMa)	–	–							
728	BZ UMa	110	30.9	6.12E–12	6.557	0.064	31.2	152	224	1.39E+07
1008	T Leo	100	31.1	9.88E–12	7.814	0.069	31.3	128	240	1.33E+07
1411	RHS40	460	32.0	3.47E–12	2.919	0.671	31.7	367	407	3.72E+07
1900	TY PsA	300:	31.7	4.68E–12	5.431	0.065	31.3	183	236	1.26E+07
1955	V405 Peg	30	29.5	3.05E–12	5.784	0.062	31.0	172	179	8.06E+06
1969	CC Scl	165	31.1	4.23E–12	4.904	0.148	31.3	203	249	1.37E+07

Notes. #713 is no longer considered non-magnetic, whereas #664 was previously classified as an IP. The luminosity is given in the ROSAT spectral band 0.1–2.4 keV. Distances and luminosities from Schwope et al. (2002) are listed in columns with tildes, all other values are from this work. V_{gen} was computed for a scale height of 200 pc.

2.2. The V/V_{max} method

We follow the approach used earlier (e.g. Hertz et al. 1990; Schwope et al. 2002; Pretorius et al. 2007) to estimate the space density of CVs using a V/V_{max} method. Since many of the CVs used here are at high galactic latitude and some of them are at a distance in excess of the likely scale height of CVs, we use the modified method by Tinney et al. (1993). This method of calculation of a generic volume, V_{gen}, accounts for an exponential density distribution $\rho \propto \exp[(-d|\sin b|)/h]$ (d: distance, b: galactic latitude, h: galactic scale height). V_{gen} is calculated by

$$V_{gen} = \Omega \frac{h^3}{|\sin^3 b|}(2 - (\xi^2 + 2\xi + 2)e^{-\xi}), \quad (1)$$

with $\xi = d|\sin b|/h$ and Ω the solid angle of the survey. The maximum generic volume V_{gen} is computed using this formula with the maximum possible distance of the particular source which would allow its detection at the flux limit of the survey. One particular CV then contributes $1/V_{gen}$ to the space density ρ_X, that is, the space density is

$$\rho_X = \sum \frac{1}{V_{gen}}. \quad (2)$$

The derived numbers per object are given in the tables below.

Per observed sample one needs to specify the flux limit, which determines the maximum distance for an object still to be detected, the scale height of the distribution, and the solid angle of the survey.

Using Gaussian distributed parallax and flux errors per object, 90% confidence regions for the derived ρ per sample and per assumed scale height were computed by running approximately 50,000 simulated mock samples per case. The results with their confidence ranges are listed in Table 4.

X-ray luminosities in this paper are always computed via $L_X = 4\pi D^2 F_X$ without any possible geometric correction factor. This leads to the revised luminosities given in the tables below.

2.2.1. The RBS sample of non-magnetic CVs

The ROSAT-sample of non-magnetic CVs described in Schwope et al. (2002) was drawn from the ROSAT Bright Survey (RBS, Schwope et al. 2000), an identification programme of all high-galactic latitude sources found in the RASS. It reached an identification rate as high as 99.7%. Based on the identification of two apparently close, low-luminosity systems, RBS0490 and RBS1955, Schwope et al. (2002) derived a space density of $\sim 3 \times 10^{-5}$ pc^{-3}. Due to their assumed proximity they were the dominating terms in the sum of Eq. (2). When the two objects were removed from their sample, the density became $\rho_{X,RBS} = 1.5 \times 10^{-6}$ pc^{-3}.

Triggered by this study, Thorstensen et al. (2006, 2009) revised the distances to RBS0490 and RBS1955 to ~300 pc and 149^{+26}_{-20} pc, respectively, thus favouring the lower value of ρ which was later confirmed by Pretorius & Knigge (2012).

The original list of RBS-CVs is given in Table 1. For a re-determination of the space density some updates are necessary. Firstly, RBS0713 (=EI UMa) is now regarded as being an IP (Baskill et al. 2005) and will not be included in the analysis. On the other hand RBS0664 was regarded as an IP previously and was re-classified as a non-magnetic CV by Pretorius & Knigge (2012).

Secondly, the RASS was recently reprocessed by Boller et al. (2016) and count rates were updated. We read the revised count rates from the online version of the catalogue[3] and convert those to fluxes using the same ECF (energy to count conversion factor) as in Schwope et al. (2002), ECF = 1.41×10^{-11} erg cm^{-2} s^{-1}/count.

Gaia distances are also listed in Table 1. All but one have errors <5%. The only exception, RBS1411, has a relative uncertainty of 23%.

The corresponding numbers for V_{gen} are listed in Table 1 together with the X-ray flux, the parallax (plus error), the

[3] http://rosat.mpe.mpg.de/cgi-bin/2RXS-funcone-search

Table 2. Non-magnetic CVs used by Pretorius & Knigge (2012) to obtain the space density of RASS-selected objects.

RBS#	Name	$\widetilde{D}$ (pc)	$\widetilde{\log L_X}$ (s^{-1})	f_X (erg cm^{-2} s^{-1})	p (mas)	Δp (mas)	$\log L_X$ (s^{-1})	D (pc)	D_{max} (pc)	V_{gen} (pc^3)
2	EF Tuc	346	31.4	1.60E–12	0.720	0.023	32.5	1335	1610	4.25E+08
22	WW Cet	158	31.2	5.70E–12	4.588	0.047	31.5	216	492	6.84E+07
280	TT Ari	335	31.7	3.50E–12	3.884	0.070	31.4	256	457	8.16E+07
288	WX Hyi	260	31.4	3.00E–12	4.273	0.029	31.3	232	383	5.03E+07
372	IQ Eri	116	30.4	1.20E–12	5.186	0.167	30.7	192	201	1.01E+07
490		285	31.2	1.60E–12	3.098	0.126	31.3	320	386	5.42E+07
512	VW Hyi	64	30.5	6.10E–12	18.531	0.022	30.3	54	127	3.40E+06
664	TW Pic	230	31.0	1.70E–12	2.284	0.022	31.6	432	537	1.42E+08
694	SU UMA	261	31.9	9.00E–12	4.535	0.029	31.7	219	626	1.97E+08
710	SW UMa	164	30.6	1.40E–12	6.148	0.080	30.6	162	183	9.24E+06
728	BZ UMa	228	31.1	2.30E–12	6.557	0.064	30.8	152	220	1.49E+07
1008	T Leo	101	30.6	3.60E–12	7.814	0.069	30.8	128	232	1.45E+07
1411	RHS40	468	31.6	1.90E–12	2.919	0.671	31.5	367	482	6.92E+07
1900	TY PsA	239	31.3	2.80E–12	5.431	0.065	31.1	183	292	2.48E+07
1955	V405 Peg	149	30.5	1.20E–12	5.784	0.062	30.6	172	179	8.92E+06
1969	CC Scl	359	31.4	1.50E–12	4.904	0.148	30.9	203	237	1.48E+07
NEP1	EX Dra	240	29.7	8.10E–14	4.058	0.019	29.8	244	491	4.93E+05
NEP2	RXJ1831	980	31.5	2.80E–13	1.232	0.038	31.3	793	2967	8.60E+06
NEP3	SDSSJ1730	444	31.2	7.30E– 13	1.864	0.038	31.4	528	3190	5.08E+06
NEP4	RXJ1715	400	30.4	1.20E–13	1.382	0.146	30.9	713	1747	3.64E+06

Notes. The luminosity is given in the spectral band 0.5–2.0 keV. Distances and luminosities with tildes are from the original publication, those without are from this work. V_{gen} was computed for a scale height of 260 pc.

Table 3. Intermediate polars used by Pretorius & Mukai (2014) to obtain the space density.

Name	$\widetilde{D}$ (pc)	$\widetilde{\log L_X}$ (s^{-1})	f_X (erg cm^{-2} s^{-1})	p (mas)	Δp (mas)	$\log L_X$ (s^{-1})	D (pc)	D_{max} (pc)	V_{gen} (pc^3)
V1223 Sgr	527	33.6	1.18E–10	1.725	0.047	33.7	571	1241	1.22E+09
V2400 Oph	280	32.7	5.00E–11	1.399	0.033	33.5	701	991	1.51E+09
AO Psc	330	32.6	3.20E–11	2.021	0.043	33.0	488	552	5.48E+07
IGR J16500	430	32.8	2.60E–11	0.855	0.062	33.6	1140	1163	2.46E+09
V405 Aur	380	32.8	3.50E–11	1.487	0.031	33.3	662	783	5.78E+08
FO Aqr	450	33.1	5.20E–11	1.902	0.051	33.2	518	747	7.76E+07
PQ Gem	510	33.0	3.10E–11	1.306	0.036	33.3	750	835	4.28E+08
TV Col	368	33.0	6.00E–11	1.951	0.018	33.3	505	782	1.94E+08
IGR J15094	960	33.5	2.60E–11	0.859	0.028	33.6	1127	1149	2.35E+09
XY Ari	270	32.5	3.60E–11	3.700	1.500	32.5	270	324	4.33E+07
EI UMa	750	33.3	2.90E–11	0.883	0.037	33.6	1095	1179	1.66E+08
NY Lup	680	33.7	9.20E–11	0.786	0.028	34.2	1228	2356	9.38E+09
V1062 Tau	1400	33.8	2.50E–11	0.632	0.077	33.8	1512	1512	2.72E+09
V2731 Oph	1000	33.9	6.90E–11	0.436	0.056	34.6	2165	3597	2.25E+09
GK Per	477	33.3	7.80E–11	2.263	0.043	33.3	437	772	7.74E+08

Notes. The luminosity is given in the spectral band 14–195 keV. Distances and luminosities with tildes are from the orginal publication, those without are from this work. V_{gen} was computed for a scale height of 120 pc.

estimated distance and the maximum distance that was used to compute the generic volume. The survey area used was 20 400 deg^2.

Here and in the other subsections the generic volume was computed for three different scale heights, that is, those that were used in the original publications: 200 pc for the RBS-CVs, 260 pc for the RASS-CVs, and 120 pc for the IPs. All derived space densities are listed in Table 4.

A few of the non-magnetic RBS-CVs might have an uncertain classification, and therefore a final composition of the sample is subject to changes if newer information becomes available. One example is RBS1955 which is difficult to classify and could well be a magnetic CV (Schwope et al. 2014); if removed from the sample, one obtains a density 10% lower than that given in Table 4.

2.2.2. The RASS (RBS and NEP) sample of non-magnetic CVs

Pretorius & Knigge (2012) used the non-magnetic RBS-CVs and added four CVs from the ROSAT-NEP (North Ecliptic Pole, Pretorius et al. 2007) survey to study the space density and the X-ray luminosity function of CVs. They re-considered all distance determinations used previously to obtain $\rho_X = 4^{+6}_{-2} \times$

Table 4. Space densities of the X-ray-selected CV samples as a function of assumed scale height.

	120 pc	200 pc	260 pc
RBS	$1.62^{+0.14}_{-0.06} \times 10^{-6}$	$1.09^{+0.11}_{-0.05} \times 10^{-6}$	$0.96^{+0.10}_{-0.05} \times 10^{-6}$
RASS	$1.09^{+0.09}_{-0.05} \times 10^{-5}$	$4.71^{+0.66}_{-0.37} \times 10^{-6}$	$3.56^{+0.58}_{-0.33} \times 10^{-6}$
RASS (RBS-part)	$1.60^{+0.17}_{-0.08} \times 10^{-6}$	$1.08^{+0.14}_{-0.06} \times 10^{-6}$	$0.95^{+0.13}_{-0.06} \times 10^{-6}$
Swift	$7.4^{+4.8}_{-1.7} \times 10^{-8}$	$3.6^{+4.0}_{-1.3} \times 10^{-8}$	$2.8^{+3.7}_{-1.2} \times 10^{-8}$

Notes. Errors are given at 90% confidence.

10^{-6} pc^{-3} for an assumed scale height of 260 pc. Their error budget is based on Monte-Carlo simulations of the probability distribution function that find ρ for a large number of mock samples with properties that fairly sample the parameter space allowed by the data.

The list of objects with their newly determined distances, luminosities, and other parameters is given in Table 2. The survey area used is 20 400 deg^2 at a limiting flux of 1.1×10^{-12} erg cm^{-2} s^{-1} for the RBS part and 81 deg^2 for the NEP part of the sample.

As a test for consistency we re-calculated the space density using their data as far as we were able to recover those. The limiting flux is not constant over the NEP area and Pretorius et al. (2007) describe how to correctly deal with the variable flux limit. It is not expected that the correct treatment makes a significant difference to the results achieved here. Following Henry et al. (2006) we therefore simply used the same limit of 2×10^{-14} erg cm^{-2} s^{-1} for the NEP survey area to obtain $\rho_{\rm X,RASS} = 4.1 \times 10^{-6}$ pc^{-3} as a reference value assuming the same scale height of $h = 260$ pc as in Pretorius & Knigge (2012).

Pretorius & Knigge (2012) used a slightly different X-ray band to Schwope et al. (2002) and corrected their fluxes for interstellar extinction which explains the different derived values of $\rho_{\rm X}$ despite using the same objects. As we show below, the differences are small compared to other parameters affecting ρ. We therefore tested the influence of the sample composition and different flux convention used by Schwope et al. (2002) and Pretorius & Knigge (2012) by removing the four NEP-CVs from the RASS-sample and re-computing the space density. The results are listed in Table 4 in the row labelled "RASS (RBS-part)".

2.2.3. The sample of intermediate polars from the *Swift*/BAT 70 month survey

The third sample to be studied here is the *Swift*/BAT sample of IPs presented by Pretorius & Mukai (2014). They list 15 IPs that were observed in the energy range 14–195 keV. This band is not affected by galactic foreground absorption. The limiting flux of this survey is $F_{\rm X} = 2.5 \times 10^{-11}$ erg cm^{-2} s^{-1} and the survey was restricted to galactic latitudes $b^{\rm II} > |5|^\circ$. The space density derived for long-period IPs with an assumed scale height of 120 pc was $\rho_{\rm X} = 1^{+1}_{-0.5} \times 10^{-7}$ pc^{-3}.

The IPs used in this exercise with their newly determined distances and luminosities are listed in Table 3.

XY Ari is behind a dark cloud and has no optical counterpart, and is therefore without data from *Gaia*. We use the same distance as Pretorius & Mukai (2014). V2731 Oph has a relative parallax error of 13%, and V1062 Tau a relative error of 12%. Most other parallax errors are below 3%.

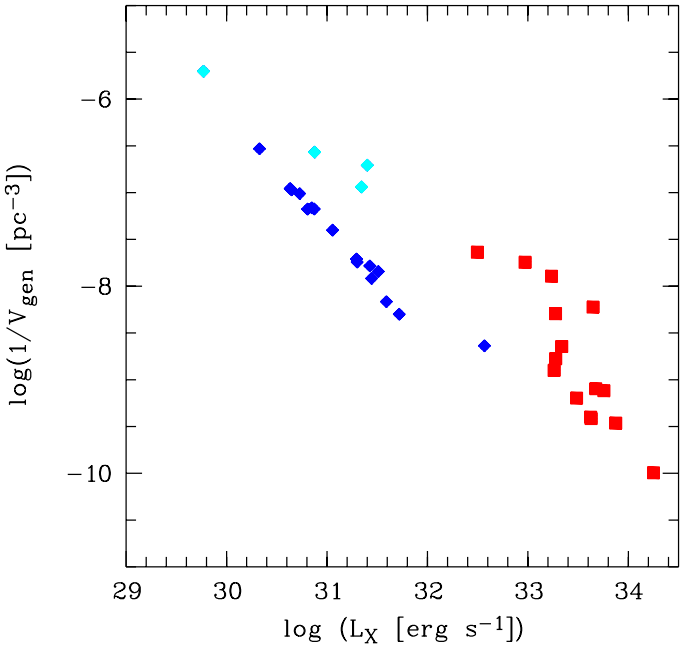

Fig. 1. Scatter plot showing the X-ray luminosities and the weights (inverse of the generic volumes) per object studied here. The *Swift*/BAT selected IPS are shown in red for a scale height of 120 pc, the RASS CVs are shown in blue, and the NEP-CVs in the RASS sample in cyan. Assumed scale height for RASS-CVs was 260 pc.

3. Results and discussion

The space densities of X-ray-selected samples of magnetic and non-magnetic CVs was redetermined using recently published parallaxes and distances from *Gaia* DR2. The results are summarized in Table 4 and Figs. 1 and 2. Figure 2 shows distributions of the original and the revised luminosities found for the RASS-CVs and the IPs, while Fig. 1 shows the weight per object (inverse of the generic volume) over its luminosity.

Just as a reference, the published values of ρ for the RBS, the RASS, and the IP samples were $\sim 1.5 \times 10^{-6}$ pc^{-3}, $4^{+6}_{-2} \times 10^{-6}$ pc^{-3}, and $1^{+1}_{-0.5} \times 10^{-7}$ pc^{-3}, for scale heights of 200 pc, 260 pc, and 120 pc, respectively (Schwope et al. 2002; Pretorius & Knigge 2012; Pretorius & Mukai 2014). The comparison with the values listed in Table 4 shows that all newly derived densities are smaller than published ones but still within the published errors.

The statistical errors of ρ of the non-magnetic CVs could be reduced very significantly thanks to precise *Gaia* data. The statistical error of ρ for the IP sample is still large due to the shallow flux limit.

For the RBS-CVs, the space density is safely below 1.8×10^{-6} pc^{-3} at 90% confidence but could be smaller than 1.1×10^{-6} pc^{-3} if the scale height were found to be as high as 260 pc as assumed by Pretorius & Knigge (2012). This result remains unchanged if the fluxes in the band 0.5–2.0 keV are used (third row in Table 4). The RBS-sample consists of long- and short-period CVs. It therefore appears possible that not all objects belong to the same galactic population. The use of just one scale to characterise the sample is likely an oversimplification.

The RASS-CVs (RBS+NEP) are compatible with a significantly higher space density thanks to the lower flux limit of the NEP. The inclusion of just four CVs from the NEP-survey implies a space density that is larger than without this inclusion by a factor ranging from 4 to 7. Figure 1 illustrates that at a given luminosity each of those CVs has a higher weight than a

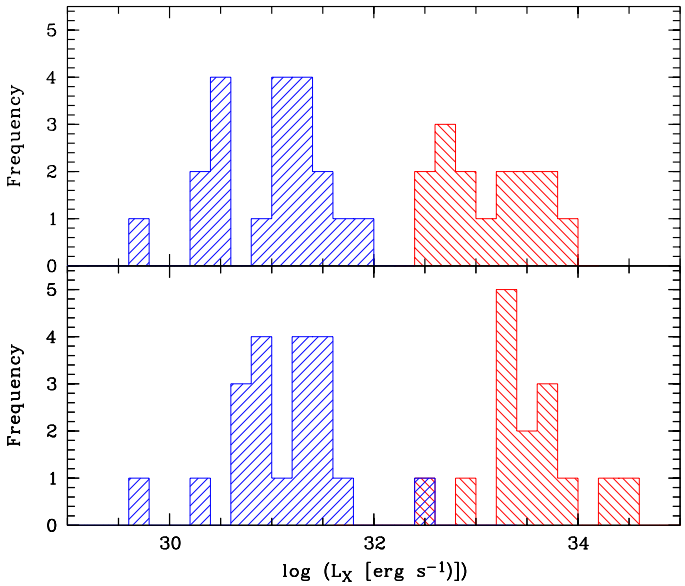

Fig. 2. Published (*upper panel*, adapted from Pretorius & Knigge 2012; Pretorius & Mukai 2014) and revised (*lower panel*) luminosity distributions of the RASS-CVs (blue-shaded histogram) and the *Swift*/BAT-selected IPs (red). The bin width is 0.2 dex.

corresponding RBS-CV by a factor of approximately ten. The whole sample is dominated by just one CV, the low-luminosity object EX Dra, $\log L_X = 29.8\,\mathrm{erg\,s^{-1}}$, a rather unhealthy situation for the whole analysis.

The pre-*Gaia* distances of the RASS-CVs were quite reliable, hence the median X-ray luminosity of the RASS sample remained unchanged at $\log L_X = 31.2\,\mathrm{erg\,s^{-1}}$. The distribution of luminosities is less dispersed in the centre but slightly more fuzzy at the outskirts (Fig. 4). The standard deviation of $\log L_X$ was 0.54 dex and is now 0.57 dex; omitting the highest and lowest values it was 0.46 dex and is now 0.38 dex.

For the IPs, the first important thing to note is that all but one object, GK Per, have larger distances than previously assumed. They are therefore more luminous than thought; the median luminosity is shifted from $\log L_X = 33.1\,\mathrm{erg\,s^{-1}}$ to $33.5\,\mathrm{erg\,s^{-1}}$. Furthermore, the survey volume becomes larger and the space density conversely smaller. An upper limit to the space density of the IPs is $\rho < 1.3 \times 10^{-7}\,\mathrm{pc^{-3}}$ at 90% confidence, a significant reduction compared to the published value. The most likely value at $7.4^{+4.8}_{-1.7} \times 10^{-8}\,\mathrm{pc^{-3}}$ is at 74% of the published one.

Distances to the IPs used by Pretorius & Mukai (2014) were either taken from the literature (3 trigonometric and 4 photometric parallaxes from the donor star) or were newly determined and based on WISE IR-magnitudes combined with the semi-empirical donor sequence by Knigge (2006). Not surprisingly, the mean distance ratio new/old is reasonably small: $d_{\mathrm{rat}} = 1.12$ for the three IPs which previously had a trigonometric parallax – among them GK Per with a *Gaia* distance smaller than published. The IPs with photometric parallaxes of the donor have $d_{\mathrm{rat}} = 1.33$ and those with estimated distances from WISE and the empirical donor sequence have a mean ratio $d_{\mathrm{rat}} = 1.74$. This leaves the two possibilities that either the IR donor sequence is somehow biased or that an additional emission component (dust, cyclotron radiation, free-free emission) mimics brighter secondaries.

Otherwise the IP sample appears more homogeneous than the sample of non-magnetic CVs. There is not one object or subgroup of objects that dominates the space density. However, given the relatively high flux limit the number for ρ derived here is valid only for the potentially rare objects with high luminosities. The putative class of low-luminosity IPs remains to be uncovered (see e.g. Worpel et al. 2018).

This present study provides an update on the space density of X-ray-selected CVs. Cataclysmic variables appear to be rarer than previously thought. While the limitations due to uncertain distances are overcome thanks to *Gaia*, major obstacles remain preventing further progress. These are the small sample sizes that are due to shallow flux limits of past X-ray surveys and a lack of information regarding the proper scale heights of the samples. It also appears likely that the existing samples are inhomogeneously composed as far as their scale height is concerned; they contain long-and short-period objects. Further, some of them lack determinations of their orbital period, which could be used to assign class membership, that is, membership of an older or younger population with corresponding scale height. The limitation caused by the small sample sizes will hopefully soon be overcome as a result of the upcoming eROSITA all-sky surveys (Merloni et al. 2012; Schwope 2012) with an all-sky flux limit comparable to the ROSAT-NEP survey but with enlarged energy coverage, 0.3−10 keV, and better spatial resolution compared to ROSAT. Performing the survey is just the first step on a longer journey, eventually involving spectroscopic identification, classification, and detailed follow-up to determine orbital periods.

Acknowledgements. I thank Fabian Emmerich for help with type-setting and Hauke Wörpel for useful hints regarding *Gaia* distances. I thank an anonymous referee whose comments helped to improve the quality and clarity of the paper. This work has made use of data from the European Space Agency (ESA) *Gaia* (`https://www.cosmos.esa.int/gaia`), processed by the *Gaia* Data Processing and Analysis Consortium (DPAC, `https://www.cosmos.esa.int/web/gaia/dpac/consortium`). Funding for the DPAC has been provided by national institutions, in particular the institutions participating in the *Gaia* Multilateral Agreement.

References

Bailer-Jones, C. A. L., Rybizki, J., Fouesneau, M., Mantelet, G., & Andrae, R. 2018, AJ, 156, 58
Baskill, D. S., Wheatley, P. J., & Osborne, J. P. 2005, MNRAS, 357, 626
Beuermann, K., & Schwope, A. D. 1994, ASP Conf. Ser., 56, 119
Boller, T., Freyberg, M. J., Trümper, J., et al. 2016, A&A, 588, A103
Henry, J. P., Mullis, C. R., Voges, W., et al. 2006, ApJS, 162, 304
Hertz, P., Bailyn, C. D., Grindlay, J. E., et al. 1990, ApJ, 364, 251
Knigge, C. 2006, MNRAS, 373, 484
Merloni, A., Predehl, P., Becker, W., et al. 2012, ArXiv e-prints [arXiv: 1209.3114]
Nobukawa, M., Uchiyama, H., Nobukawa, K. K., Yamauchi, S., & Koyama, K. 2016, ApJ, 833, 268
Pretorius, M. L., & Knigge, C. 2012, MNRAS, 419, 1442
Pretorius, M. L., & Mukai, K. 2014, MNRAS, 442, 2580
Pretorius, M. L., Knigge, C., O'Donoghue, D., et al. 2007, MNRAS, 382, 1279
Revnivtsev, M., Sazonov, S., Churazov, E., et al. 2009, Nature, 458, 1142
Schwope, A. 2012, Mem. Soc. Astron. It., 83, 844
Schwope, A., Hasinger, G., Lehmann, I., et al. 2000, Astron. Nachr., 321, 1
Schwope, A. D., Brunner, H., Buckley, D., et al. 2002, A&A, 396, 895
Schwope, A. D., Scipione, V., Traulsen, I., et al. 2014, A&A, 561, A121
Thorstensen, J. R., Lépine, S., & Shara, M. 2006, PASP, 118, 1238
Thorstensen, J. R., Schwarz, R., Schwope, A. D., et al. 2009, PASP, 121, 465
Tinney, C. G., Reid, I. N., & Mould, J. R. 1993, ApJ, 414, 254
Warwick, R. S. 2014, MNRAS, 445, 66
Webb, N. A., Schwope, A., Zolotukhin, I., Lin, D., & Rosen, S. R. 2018, A&A, 615, A133
Worpel, H., Schwope, A., Traulsen, I., Mukai, K., & Ok, S. 2018, A&A, 617, A52
Worrall, D. M., Marshall, F. E., Boldt, E. A., & Swank, J. H. 1982, ApJ, 255, 111